In-situ methane enrichment in continuous anaerobic digestion of pig slurry by zero-valent iron nanoparticles addition under mesophilic and thermophilic conditions

Míriam Cerrillo,[a] Laura Burgos,[a] Beatriz Ruiz,[a] Raquel Barrena,[b] Javier Moral-Vico,[b] Xavier Font,[b] Antoni Sánchez[b] and August Bonmatí[a]*

[a] IRTA. GIRO. Torre Marimon. E-08140, Caldes de Montbui, Barcelona (Spain).
[b] GICOM, Department of Chemical, Biological and Environmental Engineering, Universitat Autònoma de Barcelona, Edifici Q, 08193 Cerdanyola del Vallès, Barcelona (Spain).
* Corresponding autor e-mail: august.bonmati@irta.cat

ABSTRACT

The effect of zero-valent iron nanoparticles (nZVI) addition on methane production during anaerobic digestion of pig slurry was assessed. Experiments were conducted using two experimental set-ups: batch and long-term continuous operation at a fixed nZVI dosage. Two different temperature operation ranges (mesophilic and thermophilic) were assessed. Biogas production and methane content were monitored, and the specific methanogenic activity of the biomass and nZVI oxidation state were evaluated at different times. The results of batch experiments at mesophilic temperature operation showed an inhibition of methane production at all tested dosages (42, 84, 168 and 254 mg_{nZVI} g^{-1} VSS concentrations), while methane production was boosted with the lowest dosage in thermophilic temperature operation. In continuous operation, nZVI addition produced an increase in methane content of biogas, achieving values between 80-85% in both temperature ranges. The average methane production rate increased 165% and 94% with respect to the control in thermophilic and mesophilic temperature range, respectively. The oxidation state of nZVI showed a value of +3 almost immediately after contact with substrate and a slower progressive oxidation during the reactors operation. The obtained results indicate that nZVI addition in anerobic digestion is an interesting straregy for in situ biogas upgrading.

Keywords

Anaerobic digestion, nanoparticles, methane, iron zero-valent, pig slurry, biogas upgrading.

1. Introduction

Biogas is a biofuel obtained from anaerobic digestion with multiple uses since it can be directly burnt for thermal energy production or power generation. Biogas is mainly composed of methane (50-70%) and CO_2 (30-50%), and can be upgraded to natural gas grade to be suitable for other uses such as transport fuel and injection in natural gas grid [1]. Various energy demanding physical and chemical methods are used nowadays for biogas upgrading, based on CO_2 and CH_4 separation from the biogas stream, such as scrubbing, pressure swing adsorption (PSA) or membrane separation [2]. Alternatively, other technologies under development are based on the conversion of CO_2 to CH_4, such as the electromethanogenesis process that can take place in bioelectrochemical system (BES) [3].

The enhancement of methane production in anaerobic digestion is subject of constant research, and several technologies and techniques can be applied, such as bioaugmentation or co-digestion [4]. The application of nanoparticles (NPs) is receiving increasing attention as an approach to increase methane production in anaerobic digestion. NPs have been reported to be useful for wastewater treatment applications [5]. NPs could act as electron donors or acceptors and cofactor of important enzymes in various bioprocesses, which will enhance their yields [6]. The effect of different metallic nanoparticles on biogas production in anaerobic digestion has been studied, such as silver NPs on sewage sludge anaerobic digestion [7]; iron oxide (Fe_2O_3) and titanium dioxide (TiO_2) NPs on cattle manure anaerobic digestion [8]; iron oxide (Fe_2O_3) NP on two-stage anaerobic digestion with waste sludge [9]; TiO_2 NPs, on anaerobic digestion of lignocellulosic substrate [10]; magnetite and iron zero-valent, on anaerobic digestion of sludge [11]; magnetite on chicken litter anaerobic digestion [12]; or iron zero-valent, on anaerobic granular sludge [13]. Some studies have reported an inhibitory

effect of NPs, which will produce toxic effects over microorganisms, generally dosage and specific NPs dependant [14]. A previous study with nano zero-valent iron (nZVI) has reported inhibition of methanogenesis due to its disruption of cell integrity [15]. On the contrary, no ecotoxicity has been detected in other studies [16], or an increase in methane production has been reported when iron NP were added [13,17,18]. Several comprehensive reviews report the impacts of different kinds of nanoparticles on anaerobic digestion processes [6,19,20].

The use of nZVI in anaerobic digestion has been proposed as a biogas upgrading method, since it may improve the proportion of methane to the detriment of CO_2 [2]. This technique could be applied with a low investment cost and a minimum process complexity since it will not consist of CO_2 removal or adsorption (i.e. zeolites) phases, but direct CO_2 conversion into methane. In addition to biogas methane enrichment, it has been reported that biogas production is also enhanced by nZVI addition [21]. The impact of different nZVI concentrations on microbial growth has been also assessed, reporting that different conditions of substrate composition, pH or temperature produced changes in organic matter removal efficiencies [22]. Although the increasing amount of published research on the impacts of NPs on anaerobic digestion, most of the nZVI studies focus on batch and short term assays, and waste activated sludge usage. Only a few studies use high strength wastewater such as livestock manure as a substrate [21,23–25]. Short term batch investigations have reported an enhancement in methane production [26–29], while some longer term investigations showed an increase of methane production in the early stages of experiments, which is followed by an inhibition phase [30]. A methane production increase depending on NP dosage was reported in other studies [31,32].

To the extent of our knowledge, this study is the first to examine the effects of nZVI dosage onto anaerobic digestion of pig slurry on long term and continuously fed assays, and to compare mesophilic and thermophilic operation temperature conditions.

Additionally, although the effect of iron nanoparticles on anaerobic digestion has been previously reported, most of the published literature does not include much information about the behaviour of iron. In this work, the morphological and microstructural study of nZVI is presented. Furthermore, a novel study on the evolution of the oxidation state of this material when added to the anaerobic medium has been performed.

The aim of this study was to evaluate the impact of nZVI on methane production during anaerobic digestion of pig slurry, both under mesophilic and thermophilic temperature conditions, and in batch and continuous operation. Methanogenic activity tests have been applied to assess the change of microbial biomass after NP addition. Furthermore, Scanning Electron Microscope (SEM) and Electron energy-loss spectroscopy in a transmission electron microscope (TEM-EELS) have been used to monitor the morphology, microstructure and oxidation state of the NPs.

2. Materials and methods

2.1 Nanoparticles and feeding substrate

nZVI NPs were synthesised adding a sodium borohydride ($NaBH_4$, ≥98%, Sigma-Aldrich) aqueous solution to a ferrous chloride (III) ($FeCl_3$, ≥98%, Sigma-Aldrich) aqueous solution, using milli-Q grade water, based on the methodology described elsewhere [33]. Briefly, for batch assays, 200 mL of 3.72 M sodium borohydride was added dropwise to 200 mL of 0.93 M ferrous chloride while the solution was vigorously stirred under a N_2 stream at room temperature. The obtained nZVI was rinsed with milli-Q grade water and purged with nitrogen gas. The final concentration of nZVI in the stock solution was 0.47 M.

For continuous assays, to reduce the volume of stock solution added to the reactors in each pulse, the concentration of the nZVI solution was increased. A 0.93 M concentrated

105 nZVI stock solution was prepared, mixing 75 mL of 7.45 M sodium borohydride and 75 mL
106 of 1.86 M ferrous chloride with the same methodology described for batch nZVI solution.
107 The pig slurry used as feeding was collected at Puigllong farm (Gurb, Barcelona,
108 Spain), sieved (500 µm) and frozen (-20 ºC) up to its use, to assure stable composition during
109 all the experiment.
110
111 **2.2 Batch assays at different nZVI dosage**
112 Batch experiments (biochemical methane potential tests) were conducted to
113 investigate the effect of different concentrations of nZVI on the production of methane in pig
114 slurry anaerobic digestion. 120 mL serum bottles were used for this purpose, and each
115 condition was prepared in triplicate. These serum bottles were filled with a 50 g solution
116 composed of the inoculum (4 g_{VSS} L^{-1}), pig slurry as substrate (4 g_{COD} L^{-1}) and the different
117 concentrations of NP (0, 42, 84, 168 and 254 mg_{NP} g^{-1} VSS). These doses were based on
118 previous assays performed by the authors in semi-continuous AD tests of sewage sludge,
119 which had proven to be effective for methane production increase [34]. The digested sludge
120 from a mesophilic and a thermophilic lab-scale anaerobic digesters were used as inoculums
121 to test both operational temperature ranges. A control in triplicate, without pig slurry
122 substrate, was included in the setup. The bottles were sealed with rubber stoppers and capped
123 with aluminium crimp caps. The headspace was purged with N_2 for 5 min in order to remove
124 O_2 and assure anaerobic conditions. The bottles were incubated for 40 days at 37±2 ºC and
125 55±2 ºC for mesophilic and thermophilic temperature ranges, respectively. Methane
126 production was monitored periodically by taking a gas sample (0.2 mL) from the headspace
127 with a syringe and analysing the gas composition by gas chromatography.
128 Biogas was accumulated in the serum bottles headspace until the end of the assay.
129 Pressure monitoring indicated that there was no high overpressure, so microorganisms were

not affected, and it was not necessary to empty the headspace. The cumulative methane yield (V_{CH4}, mL) of each serum bottle was calculated using the N_2 concentration, which should be constant throughout the assay, to correct the molar fractions as follows (Equation 1):

$$V_{CH_4} = V_h \frac{X^0_{N_2} \cdot X_{CH_4}}{1 - X_{CH_4} - X_{CO_2}} \quad (1)$$

Where V_h is the headspace volume (mL) of the serum bottle, X^o_{N2} is the molar fraction of nitrogen measured at the beginning of the assay, and X_{CH4} and X_{CO2} are the molar fractions of CH_4 and CO_2, respectively, present in biogas determined by gas chromatography.

Pressure build-up along the assay was calculated by the increase in the number of moles determined by gas chromatography and the ideal gas equation (Equation 2).

$$PV=nRT \quad (2)$$

where P is pressure (atm), V is the serum bottle headspace volume (L), n is the number of mole of gas determined by gas chromatography (N_2, CH_4 and CO_2), R is ideal gas constant (0.082 atm L mol^{-1} K^{-1}), and T is temperature (K).

2.3 Continuous experimental set-up

Three lab-scale continuous stirred tank reactors (CSTR) were used for the experiments. Two of them were operated in mesophilic temperature range (36 ºC), and the third one was operated at thermophilic temperature range (55 ºC). The anaerobic digesters (AD) consisted of a cylindrical glass reactor (25 cm diameter, volume of 5 L) fitted with a heat jacket with hot water circulating to keep the temperature at the desired value. A temperature probe was placed into the reactor lid for temperature monitoring. Continuous mixing was supplied to each reactor using an overhead stirrer. Biogas production was measured with a gas counter (μFlow, Bioprocess Control AB, Sweden). All the digesters were already in operation, fed with pig slurry for more than a year.

155 **2.4 Reactors operation**

156 The three ADs were fed in a continuous mode with raw pig slurry with a hydraulic
157 retention time (HRT) of 10 days for the thermophilic AD and 20 days for the mesophilic ADs.
158 The pig slurry was diluted with tap water to obtain the desired organic load. The main
159 characteristics of the diluted pig slurry were as follows: total solids (TS), 29±4 g kg^{-1}; volatile
160 solids (VS), 19±3 g kg^{-1}; total chemical oxygen demand (TCOD), 36±5 g kg^{-1}; total Kjeldahl
161 nitrogen (TKN), 2.4±0.5 g kg^{-1}; ammonia nitrogen, 1.7±0.5 g kg^{-1}. The reactors were operated
162 during 265 days in 3 different phases (Table 1), with an organic loading rate (OLR) of 1.7±0.4
163 kg_{COD} m^{-3} day^{-1} and 4.1±1.1 kg_{COD} m^{-3} day^{-1} in mesophilic and thermophilic reactors,
164 respectively.

165 In Phase 1, one of the mesophilic ADs was used as control (MC), while a weekly nZVI
166 pulse of 84 mg g^{-1} SSV was injected in the second mesophilic reactor (M). In turn, the
167 thermophilic (T) reactor received a nZVI weekly pulse of 42 mg g^{-1} SSV. The dosages were
168 chosen according to the results obtained in the batch assays performed, as will be described
169 in Section 3.1. The addition of nZVI corresponding to a week was added in a unique pulse.
170 In order to compare the results of the thermophilic reactor with a control, a previous 63-day
171 period of the same reactor before starting nZVI addition was considered as Phase 0.

172 In Phase 2, a weekly pulse of nZVI was injected in the MC reactor, in the same
173 conditions as it was applied in the M reactor in Phase 1. In the case of the T and M reactors,
174 the dosages applied in Phase 2 were equal to those applied in Phase 1 but divided into 2
175 injections per week.

176 Finally, in Phase 3, NP addition was stopped in all reactors, to determine if NPs effects
177 on biogas production and its composition (richness of CH_4 and CO_2) were long lasting.

178 Each phase was maintained at least for 3 HRT to ensure a stable operation. For each
179 experimental condition, methane production rate (L_{CH4} kg_{VS}^{-1} d^{-1}) and chemical oxygen

demand (COD) removal efficiencies were used as control parameters, by taking weekly samples. Biogas composition was analysed on weekdays, to better understand the effect of nZVI addition on the anaerobic digestion process.

Table 1. Operation phases of the mesophilic control (CM), mesophilic (M) and thermophilic reactors (T).

Phase	Period (d)	Frequency of nZVI injection (times/week)			nZVI concentration of the pulse (mg_{NP} g^{-1} SSV_{added})		
		CM	M	T	CM	M	T
0	63	-	-	0	-	-	-
1	125	0	1	1	-	84	42
2	70	1	2	2	84	42	21
3	70	0	0	0	-	-	-

2.5 Specific methanogenic activities

To determine the changes in metabolic pathways when nZVI was applied, sludge samples were collected from each reactor at the end of Phase 1 and 2, and also at the end of Phase 0 in the thermophilic reactor, to perform specific methanogenic activity tests (SMA). Tests were carried out using 120 mL serum bottles, following the methodology described elsewhere [35]. A volatile fatty acid (VFA) mix (acetate/propionate/butyrate, 70/20/10), acetate, and H_2 were used as substrates. The serum bottles were filled with a 50 mL solution of the mesophilic or thermophilic sludge (1.5 g_{VSS} L^{-1}), substrate (5 g_{COD} L^{-1}), macronutrients, micronutrients and bicarbonate (1g $_{NaHCO3}$ $g_{CODadded}^{-1}$). A control duplicate without the medium was included in the set-up. The bottles were sealed with rubber stoppers and capped with aluminium crimp caps. The headspace was purged for 5 min with N_2 in order to assure anaerobic conditions. H_2 substrate addition was performed by injection of 60 mL of high purity H_2 gas (≥ 99'999%) through the septum once the serum bottle was sealed and purged. The bottles were incubated for 60 days at 37±2 ºC and 55±2 ºC for mesophilic and thermophilic temperature ranges, respectively. Methane production was monitored

202 periodically by taking a gas sample (0.2 mL) from the head space with a gas-tight syringe and
203 analysing the gas composition by gas chromatography. Biogas was accumulated in the serum
204 bottles headspace until the end of the assay, and CH_4 volume and pressure build-up were
205 calculated as described in Equations 1 and 2.

206 The SMA was calculated from the linear increase in the CH_4 concentration at the
207 beginning of the experiments (when no lag phase was observed) divided by the amount of
208 VSS.

209

210 **2.6 Analytical methods and calculations**

211 Chemical oxygen demand (COD), ammonium nitrogen (NH_4^+-N), Kjeldahl nitrogen
212 (TKN), total and volatile solids (TS, VS), total suspended and volatile suspended solids (TSS,
213 VSS), pH, total and partial alkalinity were determined according to Standard Methods 5220
214 [36]. Partial alkalinity (PA), which corresponds roughly to bicarbonate alkalinity, was
215 determined by titration with H_2SO_4 from the original pH sample to pH 5.75. Total alkalinity
216 (titration to pH 4.3) corresponds to VFA alkalinity added to bicarbonate alkalinity [37]. The
217 bulk solution pH in each sample was measured using a CRISON 2000 pH electrode. N-NH_4^+
218 and TKN were analysed by a Büchi KjelFlex K-360 distiller, and a Metrohm 702
219 SM autotitrator. Volatile fatty acids (VFA) were quantified by gas chromatography using a
220 VARIAN CP-3800 (Varian, USA) chromatograph equipped with a flame ionisation detector
221 (FID). Methane content in biogas was determined using a VARIAN CP-3800 (Varian,
222 USA) gas chromatograph equipped with a Hayesep® Q packed column (matrix 80/100) and
223 a thermal conductivity detector (TCD). A sample of 200 µL, which was taken from the
224 headspace of serum bottles (batch and SMA tests) or reactors (continuous assays) through the
225 septum, was manually injected by means of a gas tight syringe (500 µL Hamilton
226 Sampleblock Syringe) at a temperature of 180 ºC. The carrier gas was helium, with a flux of

40 mL min^{-1}. The oven and detector temperatures were set at 90 and 180 ºC, respectively. Iron concentration of the effluent and of the reactor content was determined in Phase 3 of operation by inductively coupled plasma optical emission spectroscopy (ICP-OES) (Optima 4300DV, Perkin-Elmer).

Data were analysed using one-way analysis of variance (ANOVA). Whenever significant differences of means were found, the Tukey test at the 5% significance level was performed for separation of means. Statistical analysis was performed using the R software package (R project for statistical computing, http://www.r-project.org).

2.7 Nanoparticles characterization

Samples from the content of the reactors M and T were taken during Phase 1, on day 112 to 115 of operation (M reactor) and 176 to 179 (T reactor), to characterise nZVI structure and oxidation state after a pulse. Samples were also taken during Phase 3, in order to monitor the evolution of nZVI once the pulses were stopped, on days 226, 239 and 253 of operation (mesophilic reactors) and 290, 303 and 317 (thermophilic reactor).

The characterization of nZVI in terms of size, distribution and morphology was performed using a scanning electron microscope (SEM), with a Quanta FEI 200 FEG-ESEM instrument, equipped for analysis of Energy Dispersive X-ray (EDX). A FEI Tecnai G2 F20 HR(S)TEM equipped with a Gatan Image Filter (GIF) Quantum SE 963 @ 200kV to obtain EELS spectra was also used to analyse the size, distribution and morphology of nZVI. Besides, selected areas electron diffraction images (SAED) was used to study the microstructure of the material with high resolution images. The utility for measuring the energy spectrum electron loss (EELS) was used to obtain information about the oxidation state of nZVI.

The EELS spectra defines a L_{32} ratio, which corresponds to a defined oxidation state of iron according to Tan et al [38]. According to them, a value of 2.99 of this ratio corresponds to zerovalent iron, while oxidation states of +2 and +3 correspond to 3.99 and 4.55 L_{32} values respectively. Two different types of tests were performed for comparison: test number 1 consisted in studying nZVI evolution in a batch test using a 25 mL hermetically closed and nitrogenized bottle. This test was performed with two combinations: test 1a) nZVI in an aqueous suspension up to 14 days, and test 1b) nZVI added to anaerobic inoculum + pig slurry (anaerobic medium) at the same concentration of continuous reactors up to 7 days. In test number 2, nZVI samples were collected from continuous reactors operated up to three days: test 2a) mesophilic reactors, and test 2b) thermophilic reactors.

3. Results and discussion

3.1 Methane production in batch assays at different nZVI dosage

Specific methane productions and initial slopes obtained in the batch assays under mesophilic and thermophilic conditions are presented in Figure 1. For both temperature ranges, maximum specific methane productions were obtained with no NP addition (267.6 and 235.0 L_{CH4} kg_{VS}^{-1} for mesophilic and thermophilic operation, respectively). Under mesophilic conditions, increasing nZVI concentration decreased methane production. Differently, under thermophilic conditions, the concentrations of 0 and 42 mg_{NP} g^{-1} VSS achieved similar methane production, with no significant statistical differences ($p < 0.05$). Interestingly, all NP concentrations boosted methane production during the first 20 days of the thermophilic batch assay, as it is shown by the initial slopes. Figure S1 shows the accumulated methane production of the different tested conditions. It is difficult to compare the obtained results with previous reports because of the different ways of expressing NP dosage. Most studies report the dosage in terms of volume (mg L^{-1}), when in other works it is

preferred to express it as a function of the organic matter present in the substrate, as stated by Lizama and coworkers [39]. The nZVI concentrations tested in this assay were between 2.5 and 15.4 mM, and previous works have reported an inhibition of methanogenic activity with increasing concentrations of nZVI in mesophilic glucose anaerobic digestion (in a range of 1 to 30 mM) [15]. Other work has reported an increase in specific biogas and methane production in cattle manure batch mesophilic anaerobic digestion when increasing nZVI concentrations from 5 to 20 mg L^{-1} [21]. Batch assays with poultry litter and nZVI at 15, 50 and 100 mg L^{-1} (1.68, 5.58 and 11.17 mg_{NP} g^{-1} VS) increased methane production up to 29.1% compared to no nZVI addition [24]. Finally, adding 9 mg_{NP} g^{-1} VS to sewage sludge mesophilic anaerobic batch assays increased biogas yield and methane content 135% and 186%, respectively, with respect to control [39]. The concentrations of these assays are also lower than the ones tested in this assay, which range from 140 to 860 mg L^{-1}.

Wu and coworkers (2015) tested ZVI in batch anaerobic digestion of swine manure, although using powder form instead of NP, with concentrations as high as 50 g L^{-1}. It was reported that although methane production increased with the applied dose, excessive ZVI doses did not stimulate methane production further and probably exerted negative effects on microbial activity [40]. The addition of 5 g L^{-1} of ZVI powder to ammonia-rich swine manure batch anaerobic digestion was reported to achieve 54.2% higher methane yield relative to control [41].

This batch assay results show a clear inhibition of methane production in mesophilic temperature conditions and an initial methane boost in thermophilic conditions, which may be due to an excessive dosage compared to other works. Other possible inhibition causes in batch assays are discussed later in Section 3.2.4.

Regarding the different behaviour between mesophilic and thermophilic conditions, it has been reported previously and improvement in COD removal efficiency when increasing

AD temperature from 37 ºC to 50 ºC with a 50 g L^{-1} addition of nZVI (13.37% and 33.43%, respectively), while the control reactor reduced its activity with the increase of temperature [22]. Furthermore, in this study, the thermophilic inoculum used in batch assays was obtained from the thermophilic reactor used in continuous operation mode. This reactor had been operated in previous assays with high organic and nitrogen loading rates, and hydrogenotrophic methanogens represented a high proportion of methanogenic archaea [42]. Biomass may be better acclimated and able to shift to hydrogenotrophic methanogenic metabolic pathway compared to the mesophilic temperature reactor, as the results of the SMA test have also shown (Section 3.3).

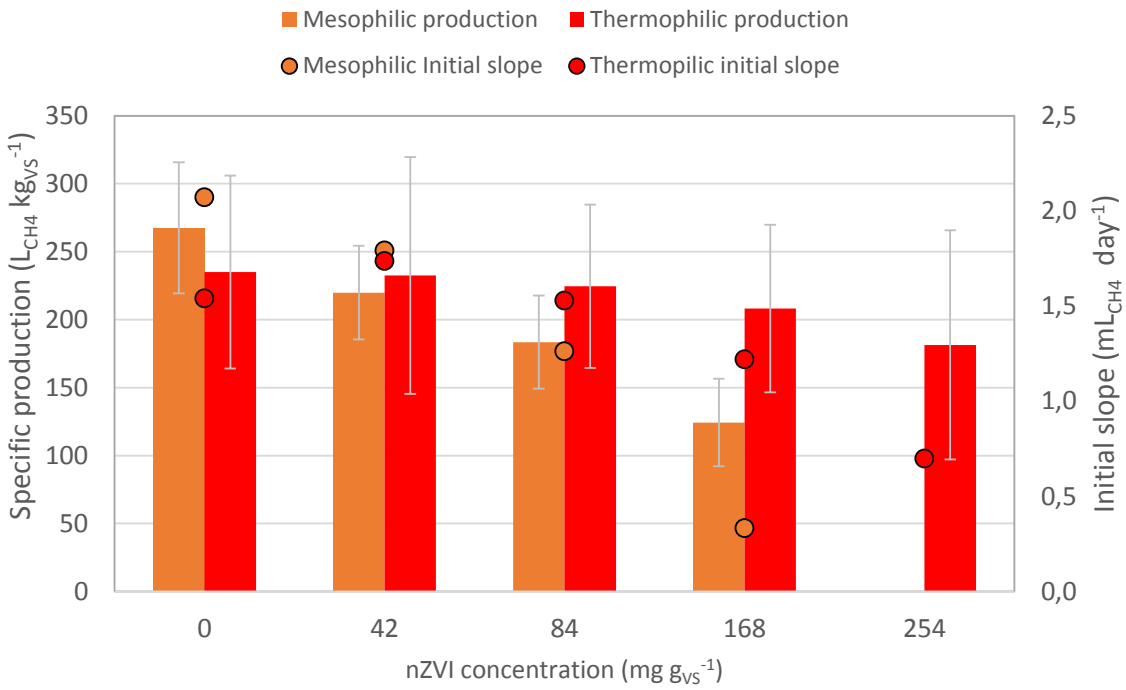

Figure 1. Specific methane production and initial slope of the batch assays performed in mesophilic and thermophilic temperature conditions with different nZVI dosages.

Although batch assays results have not shown a clear improvement in methane production, previous assays of the group in semi-continuous operation mode had proven to increase methane production in AD of sewage sludge in the tested dose range [34]. Consequently, the doses chosen to be tested in continuous operation assay were in the low

concentration range, 84 and 42 mg_{NP} g^{-1} VSS_{added} for mesophilic (M) and thermophilic (T) reactors, respectively, to test if inhibition could be avoided in continuous operation mode, and to be able to compare the results obtained in both operation modes. Furthermore, continuous operation mode could have an acclimation effect on the biomass that may result in different behaviour of the anaerobic digestion process compared to batch tests [34].

3.2 Methane production in continuous assays with nZVI addition

3.2.1 Thermophilic temperature range operation

An increase in the content of methane in the biogas was produced with nZVI addition in continuous anaerobic digestion. As shown in Figure 2a, the percentage of methane in the thermophilic reactor increased from 64% in Phase 0 to a maximum value of 87% in Phase 1. Methane content showed an increase after each weekly pulse of nZVI, which was maintained for several days, followed by a decrease, until a new pulse was added. The boost in methane content was produced shortly after the nZVI pulse was added to the reactor (in the range of hours), as shown in the inset of Figure 2a. Previous work has reported that more than 90% of the total H_2 volume delivered by nZVI was produced in the first hour, regardless of initial nZVI concentration [43]. The same authors described that nZVI is easily deactivated during the dissolution process because of the formation of iron-related precipitates on its surface, due to its strong reducing power, resulting in much slower H_2 production rates after the first hour of dissolution.

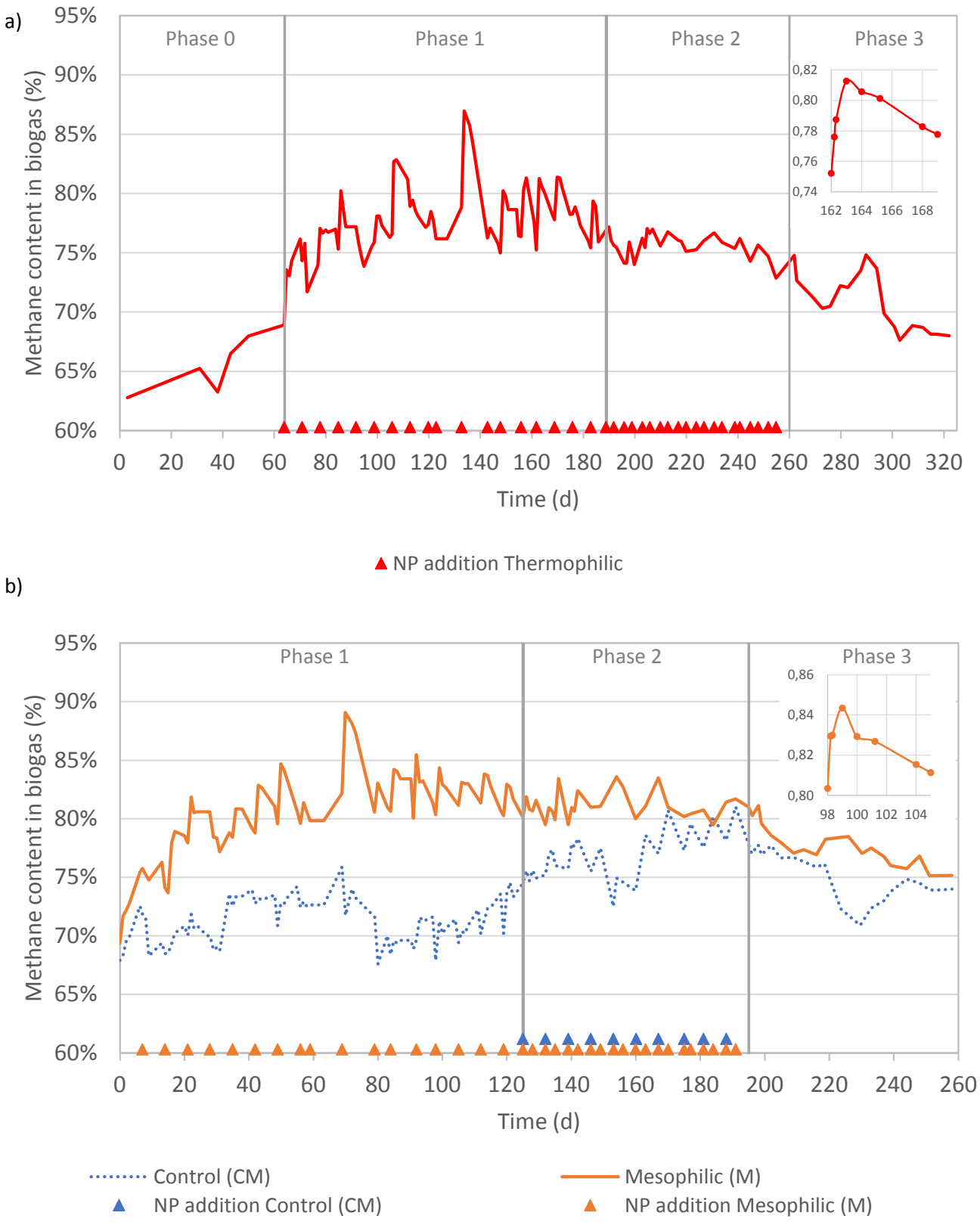

Figure 2. Methane content in biogas in the different phases of operation in a) thermophilic temperature conditions in reactor T (detail in the inset of the peak from day 162 to 169); b) mesophilic temperature conditions in reactors CM and M (detail in the inset of the peak of M reactor from day 98 to 105).

346 During Phase 2, when the weekly dosage was split into two pulses per week, the peaks
347 were of less magnitude, but the average value was maintained (Table 2). With the nZVI pulses
348 suppression, in Phase 3, the methane content in biogas showed a sustained decrease, returning
349 to values that were similar to phase 0. This behaviour shows that the nZVI accumulated in the
350 reactor in the previous phases has a delayed background effect on the operation. Previous
351 studies have shown the long-lasting effect of nZVI, since depending on the degree of
352 crystallinity of the particles, complete oxidation of Fe(0) could last between two weeks and a
353 year [44,45]. Indeed, Fe concentration evaluation during Phase 3 (Figure S2) showed that
354 0.45 mg_{Fe} g^{-1} were still present in the effluent 10 days after the last nZVI pulse. The effluent
355 and reactor content Fe concentration decreased to 0.05 mg_{Fe} g^{-1} 65 days after the last pulse,
356 following the biogas methane content decreasing tendency during Phase 3. The fate of nZVI
357 after being corroded to Fe^{2+} in the anaerobic digester is probably the formation of insoluble
358 siderite ($FeCO_3$), by interaction with CO_2; or the precipitation with PO_4^{3-} to form vivianite
359 ($Fe_3(PO_4)_2$), as described in both cases by Puyol and co-workers (2018) [46].

360

361 **Table 2.** Main operational results of the three reactors, mesophilic control (MC), mesophilic
362 (M) and thermophilic (T) in the different phases (mean±standard deviation).

Phase	Reactor	Methane content in biogas (%)	Methane production (L kg_{VS}^{-1} d^{-1})	COD removal (%)	pH	Total Alkalinity (g $CaCO_3$ L^{-1})	Partial Alkalinity (g $CaCO_3$ L^{-1})
1	CM	71±2	214±78	50±9	8.1±0.2	7.2±0.8	6.5±0.9
2		77±2	404±100	46±11	8.2±0.1	10.7±1.4	9.4±1.3
3		75±2	342±88	49±11	8.3±0.1	11.1±1.0	9.8±0.7
1	M	81±4	255±85	48±10	8.3±0.1	7.6±1.2	6.7±1.0
2		81±1	402±128	45±12	8.5±0.3	10.3±1.2	8.8±1.1
3		78±2	321±118	52±15	8.4±0.1	10.8±0.7	9.9±0.6
0	T	66±2	65±22	31±10	8.2±0.1	9.2±0.9	7.6±0.8
1		78±3	140±57	40±10	8.2±0.2	6.4±0.7	5.6±0.6
2		76±1	172±56	45±13	8.4±0.1	9.7±1.0	7.7±1.0
3		71±2	146±54	50±9	8.2±0.1	9.1±1.2	7.7±0.9

363

364 The average methane production rate increased 165% during the nZVI application
365 phases, from 65±22 to 172±56 $L_{methane}$ kg_{VS}^{-1} d^{-1} (Table 2, Figure S3). Finally, no significant
366 statistical differences were found in the COD removal efficiency in any operational phase,
367 which presented averages in a range between 31% and 50% (Table 2). Since no significant
368 increase in COD removal efficiency was observed, the increase in methane production may
369 be due to hydrogenotrophic methanogens H_2 (produced by nZVI corrosion) uptake and
370 reaction with CO_2.
371
372 **3.2.2 Mesophilic temperature range operation**
373 Regarding the mesophilic reactors, a clear increase in methane content in biogas of M
374 reactor compared to control (MC) was produced in Phase 1 (Figure 2b). Values of 88% were
375 reached in M reactor, while methane content in MC was in a range of 67-69%. As in the
376 thermophilic reactor, the increase of methane content was produced some hours after the pulse
377 and was followed by a decrease at the end of the week.
378 When nZVI was added also to CM reactor (Phase 2), the methane content of biogas
379 increased and reached the values obtained in the M reactor, over 80% during the peak. On the
380 other hand, reactor M showed a more stable methane content value when the dosage was
381 divided into two pulses a week (Figure 2b).
382 In Phase 3, methane content percentages started to decrease in both reactors in a steady
383 way, as described for the thermophilic reactor. Fe concentration in mesophilic reactors during
384 Phase 3 (Figure S2) showed higher values compared to T reactor, since the HRT was double
385 than in T reactor. Fe concentration was the highest in M reactor, maybe due to differences in
386 mixing efficiency compared to CM reactor. The effluent of M and CM reactors contained 1.5
387 and 0.9 mg_{Fe} g^{-1}, respectively, 10 days after the last pulse, which decreased to 0.48 and 0.18
388 mg_{Fe} g^{-1} on day 65. Fe concentration in the effluent in Phase 3 correlates well with the slightly

389 higher methane content of M reactor compared to CM reactor, and the faster decrease
390 observed in T reactor.

391 The methane production rate average values in Table 2 show that reactor M produced
392 20% more methane during Phase 1 than reactor CM, with a total increase of 94% in Phase 2.
393 The methane production of both reactors was similar in Phase 2, when CM reactor was
394 submitted to nZVI addition, with a 94% improvement in the CM reactor (Figure S2). The
395 COD removal efficiencies were similar in both reactors in all the phases, as shown in Table
396 2, similar to the behaviour described for the thermophilic reactor.

397

398 **3.2.3 Other operation parameters evolution**

399 Regarding other control parameters, data corresponding to pH, alkalinity and VFA is
400 presented as Supporting Information. pH of the 3 reactors oscillated in general between 8.0
401 and 8.5 (Figure S4a and Figure S5a). Other authors have reported inhibition of the AD process
402 at pH over 8.0 [47,48], but in this study, reactors performed in a stable way in all the operation
403 time. An increase in pH has been reported due to the consumption of bicarbonate by
404 hydrogenotrophic methanogens [48]. Previous research articles have reported that pH may
405 increase or remain stable with the addition of nZVI, according to Equations 3 and 4 [22,49].

406

407 $$4Fe_0 + 8H^+ + CO_2 \dashrightarrow 4Fe^{2+} + CH_4 + 2H_2O \quad (3)$$

408 $$Fe_0 + 2H_2O \dashrightarrow Fe^{2+} + H_2 + 2OH^- \quad (4)$$

409 In this study, no significant statistical differences have been observed comparing CM
410 and M reactor pH or the different operation phases (Table 2). Regarding TA and PA, all
411 reactors showed an increase in Phase 2 (Figure S4b and Figure S5b-c), that can be related to
412 the increase in VFA of the influent in this phase (Figure S4c-d and Figure S6). This increase

413 in the VFA content of the influent may also explain the temporal accumulation of acetic and
414 propionic acid in this phase, rather than being produced by methanogens inhibition.
415
416 **3.2.4 Influence of AD operation mode on nZVI effect**
417 The observed improvement in methane production in continuous operation mode may
418 be due to different nZVI effects. On the one hand, the release of hydrogen during nZVI
419 corrosion/oxidation (Equation 3) can serve as the electron donor for methanogens [13,50],
420 activating hydrogenotrophic metabolic pathway (Equation 5); and homoacetogens, for the
421 production of acetic acid (Equation 6), which in turn could be converted into methane by
422 acetoclastic methanogens (Equation 7) [51].
423
424 $$4H_2 + CO_2 \rightarrow CH_4 + 2H_2O \quad (5)$$
425 $$4H_2 + 2CO_2 \rightarrow CH_3COO^- + H^+ + 2H_2O \quad (6)$$
426 $$CH_3COO^- + H^+ \rightarrow CH_4 + CO_2 \quad (7)$$
427
428 On the other hand, nZVI may facilitate electron conduction. Several studies have
429 shown that iron nanoparticles can accelerate direct interspecies electron transfer (DIET) [52]
430 between bacteria and methanogens [53]. Other relative larger conductive materials that have
431 been tested in AD, such as biochar [54] or granular activated carbon [55,56] may be used by
432 syntrophic microorganisms as an attaching surface. Differently, NPs attach to conductive pili,
433 reducing the requirement of multi-heme *c*-type cytochromes for DIET [53].
434 The activity stimulation of key enzymes related to hydrolysis and acidogenesis has
435 been reported in the AD of waste activated sludge (WAS) [57]. Hydrolysis of organic
436 compounds to soluble substances is the rate-limiting step of AD when complex particulate
437 organic matter predominates in the substrate.

438 Finally, nZVI may also react with toxic substances in the reactor, such as ammonia
439 nitrogen [5,41] or hydrogen sulphide (H_2S) [24], lowering their concentration and alleviating
440 inhibition phenomena on acetogens and methanogens.

441 The different behaviour of anaerobic digestion process observed in batch and
442 continuous assays in this study may be due to an excess concentration of nZVI in relation to
443 the total volume of the vial and reactors. The applied dosage was related to the amount of
444 VSS that were added with the feeding. In the case of the continuous operation, each weekly
445 pulse contributed to 0.6-0.7 g_{NP} L^{-1} with respect to the total volume of the reactor at the
446 moment of application, which is in the range of the higher dose tested in batch assays. But, if
447 this amount was distributed along the week, it would correspond to a concentration of 86-103
448 mg_{NP} L^{-1}. These values are in the range of the successful concentrations used in the studies
449 referenced in the batch assays section.

450 Furthermore, in batch assays, the released H_2 by corrosion of nZVI could accumulate
451 in the headspace due to rapid nZVI dilution and produce inhibition, accompanied by reductive
452 decomposition of cell membrane [43]. Furthermore, the possible increase of pH described in
453 Equation 3 or a possible accumulation of VFA due to the improvement of hydrolysis step [57]
454 may have adversely impacted methanogenesis in batch operation, while fresh substrate
455 addition may have helped to alleviate this effect in continuous operation [58].

456

457 **3.3 Specific methanogenic activity**

458 SMAs of the biomass of the three reactors were determined at the end of Phase 1 and
459 Phase 2, besides Phase 0 in T reactor (Table 3, Figure S3). M reactor showed lower SMA
460 values for all substrates than CM reactor, except for SMA_{H2} in phase 2. SMA values of CM
461 reactor also decreased in Phase 2, when nZVI was added. Using the VFA mix as a substrate
462 decreased the SMA in comparison to the acetic acid substrate in mesophilic temperature

conditions in both reactors. This reduction may be due to an inhibition of propionate or butyrate degrading bacteria. No inhibition of the acetoclastic methanogenesis metabolic pathway has been detected, corroborating the fact that the accumulation of acetic acid during Phase 2 was not due to acetoclastic methanogens inhibition.

Table 3. Specific methanogenic activity (SMA) at the start of the assay (Phase 0), and end of Phase 1 and Phase 2 of the biomass of mesophilic control (MC), mesophilic (M) and thermophilic (T) fed with different substrates. ND: not determined.

Phase	Reactor	SMA (mg COD_{CH4} g_{VSS}^{-1} day^{-1})			
		VFA mix	Acetate	H_2	Blank
1	CM	198	281	22	1
2		156	210	16	1
1	M	111	239	11	2
2		71	209	22	4
0	T	189	ND	27	6
1		193	103	83	2
2		120	218	71	3

Regarding T reactor, it showed a higher SMA value with H_2 substrate than the one obtained for mesophilic reactors, which suggests better acclimatisation. The addition of nZVI boosted SMA with acetic acid and H_2 substrates, which produced a 2-times increase from Phase 1 to Phase 2 and a 3-times increase from Phase 0 to Phase 1, respectively. On the contrary, the VFA mix SMA was reduced 36% from Phase 0 to Phase 2. The activation of the hydrogenotrophic metabolic pathway correlates well with methanogens using hydrogen released during nZVI corrosion/oxidation as an electron donor.

Although the evolution of the SMA_{H2} in T reactor correlates well with the improvement shown in continuous operation, and the possibility that H_2 production by nZVI corrosion may enhance hydrogenotrophic metabolical pathway, the results obtained in M reactor compared to CM reactor are not so conclusive. As it has been shown by the results of the continuous assays, the effect of nZVI addition on methane production is especially remarkable a few hours after the pulse. Therefore, once the pulses were suppressed in Phase

485 3, the system returned slowly to the initial values. Furthermore, Fe oxidation may accelerate
486 once the inoculum is exposed to air for assay preparation. Therefore, the effect of nZVI on
487 biomass may have diluted during the SMA assays.
488
489 **3.4 Morphologic and microstructural characterisation of nZVI**
490 The SEM images obtained for the morphological characterization of nZVI showed the
491 typical aggregation that occurs due to the existence of Van der Waals forces [59] (Figure 3a).
492 The size of the observed particles, which describe spherical formations, were between 10 and
493 20 nm in diameter (Figure 3a). This aggregation was observed in TEM with a worm-like
494 shape (Figure 3b). These formations for the nZVI observed with TEM are widely described
495 in the literature [60]. It is clearly observed, as well, how once the oxidation process of NPs
496 begins, a needle configuration on the outside is formed, configuring a rough morphology of
497 these as observed in Figure 3c, which may be due to the formation of iron oxides and
498 oxohydroxides [61]. These formations can also be seen in TEM images (Figure 3d, e), as
499 mentioned in the next section on oxidation of Fe NPs. TEM images also showed the contact
500 between nZVI and bacteria present in the reactors (Figure 3f).
501 A high resolution TEM image (Figure 3g) and an electron diffraction image of selected
502 areas (SAED) (Figure 3h) revealed the existence of iron microcrystals with crystalline planes
503 belonging to phases existing in the sample like the α phase of iron, and other iron oxides
504 phases. It is very likely to have iron oxohydroxides of the FeOOH type, which cannot be
505 identified with this technique due to their amorphous nature. All the analysed images
506 presented a typical interplanar distance of the α-Fe of about 0.21 nm [62]. Other typical
507 interplane distances of some iron oxides such as 0.14 nm and 0.25 nm [61] can be observed
508 as well, which indicates that a part of the analysed samples presents a certain degree of
509 oxidation, and therefore the coexistence of oxidized and unoxidized Fe. This fact coincides

510 with the hypotheses raised in the literature [62], which state that oxidized and unoxidized
511 areas coexist, and oxidation occurs in the external parts of the nanoparticle, as confirmed in
512 the next section of this work. The plane distances found in all the samples analysed are very
513 similar, with very little variability among them.
514

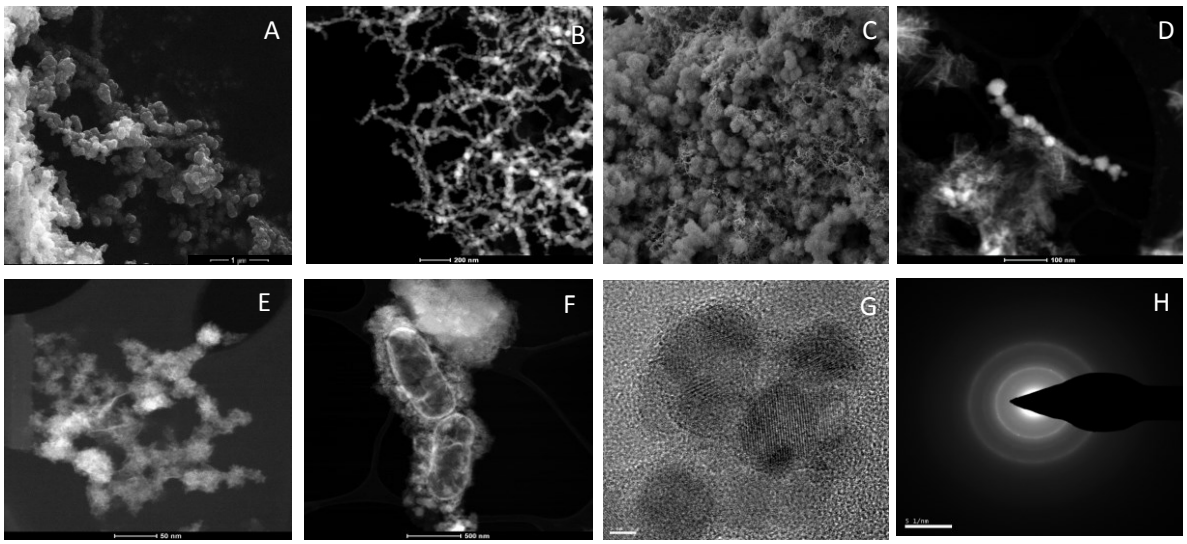

515
516
517 **Figure 3.** SEM images of: a) freshly synthesized nZVI, c) nZVI one day after synthesis; TEM
518 images of: b) freshly synthesized nZVI, d) nZVI one day after synthesis, e) nZVI from a
519 thermophilic reactor 10 min after addition, f) nZVI-bacteria contact in a nitrogenised bottle
520 (test 2), in the 6th day after addition, g) high resolution image of freshly synthesized nZVI, h)
521 SAED pattern of freshly synthesized nZVI.
522

523 **3.5 Oxidation state evolution of nZVI**

524 The evolution of the oxidation states of nZVI over the days based on the information
525 on the L_{32} index can be seen in Table 4. The time scale observed in Table 4 starts when nZVI
526 is added to the bottle containing water (test 1a), anaerobic medium (test 1b), or to the
527 continuous reactors (tests 2a, b), and day 1 means that the sample is taken 24 hours later. As
528 seen, within the experimental variability, the oxidation state of nZVI in test 1a) is maintained
529 up to 14 days at L_{32} values of around 4, which corresponds to a +2 oxidation state of iron.
530 Right after synthesis, nZVI is a little oxidized, but L_{32} ratio (3.3) is near theoretical 2.99
531 corresponding to a zerovalent oxidation state. It can be stated that from the first day after the

synthesis, particles increase their oxidation state to +2. However, the L_{32} ratio does not go beyond 4.2 after 14 days of the synthesis, which corresponds to an oxidation state between +2 and +3. This fact contrasts with the oxidation state evolution observed when nZVI is added to anaerobic medium both in tests 1b) and 2a, b), which entails an immediate oxidation to a +3 state, a level that was not reached even after 14 days when nZVI is in an aqueous suspension. In fact, only 10 minutes were necessary to reach that level of oxidation, which indicates that this process happens very quickly once nZVI comes into contact with anaerobic medium. The three tests (1b, 2a, 2b) performed including nZVI and anaerobic medium show very similar behaviour in terms of oxidation state evolution, with slightly faster oxidation for real reactors, even a little faster in the case of the thermophilic reactor, agreeing with the fact that higher temperatures normally accelerate reactions. Besides, L_{32} ratio indicates a +3 oxidation state is reached immediately, and it does not stop growing during the development of the test, which indicates that nZVI has oxidation capacity beyond +3, which agrees with the statement mentioned in section 3.2.1 about the long-lasting oxidation of nZVI.

Table 4. L_{32} ratio data used for the evaluation of the oxidation state of nZVI in several tests up to 14 days.

	Day							
Oxidation State Evaluation Test	**0 – 10 min***	**0 – 60 min**	**1**	**2**	**3**	**6**	**7**	**14**
1a) nZVI	3.3	-	4.0	3.7	4.0	3.4	4.2	4.0
1b) nZVI+Substrate	4.5	4.7	4.7	5.2	5.4	6.0	6.7	-
2a) Mesophilic Reactor	4.8	-	5.2	-	5.7	-	-	-
2b) Thermophilic Reactor	4.7	-	5.4	-	5.9	-	-	-

*EELS Spectra in test 1a was only evaluated 10 minutes after synthesis, time scale for tests 1b, 2a and 2b starts at the moment nZVI is added to anaerobic medium.

Regarding the effects of oxidation state on morphology, two differentiated areas can be observed in all samples, one with spherical iron NPs (Figure 3a) that are normally linked with worm-like shapes observed in TEM images, as already mentioned in the previous section

555 (Figure 3c), and another area of needle-shaped material, which usually corresponds to species
556 of iron oxides and oxohydroxides (e.g. $FeCO_3$, Fe_3O_4, Fe_2O_3, $Fe(OH)_3$ and FeOOH) [61],
557 which is confirmed by the fact that these latter areas are always more oxidized than the others
558 when analysing their L_{32} index. These two areas normally coexist, as observed in Figure 3d.
559 It is also observed that the areas of needles are more numerous as the test progresses and that
560 their degree of oxidation increases quite consistently throughout the days. Thus, needle shapes
561 are scarcely observed in samples of freshly synthesized NPs, but their presence increases as
562 the tests proceed. In addition, the images reveal that nZVI oxidation starts at the surface of
563 the nanoparticles, which causes their hairy appearance as the oxidation proceeds (Figure 3e).
564

565 **3.6 Evaluation of anaerobic digestion with nZVI addition**

566 Although previous works have shown an improvement of methane yield with the
567 addition of nZVI in batch AD of livestock manure, as described in section 3.1, to the authors'
568 knowledge no continuous long-term operation assays have been reported. Different substrates
569 have been used in previous studies in continuous operation. However, the specific
570 characteristics of each substrate, such as pH, TS/VS, alkalinity or ammonia content, may
571 change the effect of nZVI addition [22]. Furthermore, in those studies ZVI is used in different
572 formats, such as scrap or iron powder. As particle size decreases, the surface-to-volume ratio
573 increases, probably changing the properties of the material [63]

574 Previous studies in semi-continuous mode mesophilic AD of sewage sludge have
575 reported an increase in methane content in biogas from 65.1% to 75.9% when dosing of 0.81
576 g L^{-1} nZVI every seven days [34]. An increase from 60 to 75% was achieved by digestion of
577 palm oil mill effluent with 16 g L^{-1} ZVI powder addition under mesophilic conditions [58].

578 Compared to other in-situ biological upgrading techniques applied to livestock
579 manure, such as H_2 external addition, the final methane content in biogas in this study is above

580 the results reported in other works. For example, Luo and co-workers (2012) reported 65%
581 methane content when digesting cattle manure with direct addition of H_2 to the reactor [48],
582 while Luo and Angelidaki (2013) reported 75% methane content when co-digesting cattle
583 manure and whey in thermophilic conditions with the same biogas upgrading technique [47].
584

585 **3.7 Economic and environmental challenges for nZVI addition to AD**

586 The results obtained in this study show an improvement of methane production in
587 continuous long-term anaerobic digestion operation. The achieved biogas methane content is
588 near the values required for methane injection in the natural gas net. In this sense, an
589 adjustment of nZVI dosages is needed in order to determine if natural gas quality grade can
590 be achieved, in order to avoid further upgrading steps. This partial CO_2 conversion in the
591 biogas would decrease upgrading costs if methane content needed further increase. In a
592 moment when great efforts are being made to upgrade biogas according to its methane
593 content, this strategy supposes a clear decrease in the environmental and economic impact of
594 these processes. Furthermore, by nZVI addition method, the total methane mass is increased,
595 differently to other physical or chemical biogas upgrading technologies based on CO_2
596 removal. Furthermore, such as other biological technologies, the process is performed at mild
597 operational conditions, at moderate temperature levels and atmospheric pressure, contributing
598 to the sustainability of the technique [1].

599 However, up to now in-situ nZVI addition to AD is not competitive compared to
600 established biogas upgrading techniques. nZVI production methods must ensure the
601 efficiency of the obtained NPs and be able to produce them at a large scale while maintaining
602 the reproducibility in size and chemical composition. The critical point for nZVI production
603 is the cost of $NaBH_4$. It has been reported that the cost of nZVI production was of 0.95€ g^{-1},
604 where $NaBH_4$ reactant represented 85% of this cost [64]. In order to be applicable at a large

605 scale, nZVI cost has to be decreased, i.e. by using extracts obtained from natural products,
606 such as leaves from oak trees [64] or alternative methods such as precision milling [65].
607 Further process costs reduction could be achieved by using waste streams as Fe source. Iron
608 nanoparticles have been successfully biosynthetized from water treatment sludge, so the use
609 of commercial chemical precursors with analytical grades (e.g. $FeSO_4$, $FeNO_3$ and $FeCl_2$)
610 could be avoided [18]. The evaluation of the purity of these nanoparticles should be addressed,
611 besides their efficiency in AD application for methane enhancement.

612 Finally, nanoparticles use may present an environmental challenge that needs to be
613 evaluated. Life cycle assessment (LCA) of the use of different metallic nanoparticles in
614 anaerobic digestion of manure has been recently performed [66]. That study reported that
615 anaerobic digestion supplemented with NP reduced greenhouse gas emissions, acidification,
616 eutrophication, resource depletion, ozone layer depletion potential and human toxicity
617 potential compared with no supplemented process.

618

619 **4. Conclusions**

620 Batch and continuous assays have been performed in order to evaluate nZVI addition
621 to anaerobic digestion of pig slurry, both in mesophilic and thermophilic temperature ranges.
622 Long term continuous assays have shown a clear enhancement in methane content in biogas,
623 in addition to an increase in methane production rate, while results in batch assays were less
624 conclusive probably due to a low acclimation of microorganisms. Methane content in biogas
625 in continuous operation achieved 88% and 87% in mesophilic and thermophilic conditions,
626 respectively. The average methane production rate increased 165% and 94% with respect to
627 the control in thermophilic and mesophilic temperature range, with nZVI dosages of 42 mg
628 g^{-1} SSV and 84 mg g^{-1} SSV, respectively. nZVI showed rapid oxidation when mixed with the
629 substrate, although the oxidation process was maintained at least for one week. Compared to

conventional techniques for biogas upgrading, in situ nZVI addition would represent a decrease in investment and operation costs, although the reduction of nZVI production cost must be achieved. Furthermore, CO_2 would be converted in CH_4, instead of removed, increasing the final methane production.

Conflicts of interest

There are no conflicts to declare.

Acknowledgements

This research was funded by the Spanish Ministry of Economy and Competitiveness (INIA project RTA2015-00079-C02-01). The support of the CERCA Program and of the Consolidated Research Group TERRA (ref. 2017 SGR 1290), both from the Generalitat de Catalunya, is also acknowledged.

References

[1] I. Angelidaki, L. Treu, P. Tsapekos, G. Luo, S. Campanaro, H. Wenzel, P.G. Kougias, Biogas upgrading and utilization: Current status and perspectives, Biotechnol. Adv. 36 (2018) 452–466. https://doi.org/https://doi.org/10.1016/j.biotechadv.2018.01.011.

[2] D. Dong, P. Aleta, X. Zhao, O.K. Choi, S. Kim, J.W. Lee, Effects of nanoscale zero valent iron (nZVI) concentration on the biochemical conversion of gaseous carbon dioxide (CO2) into methane (CH4), Bioresour. Technol. 275 (2019) 314–320. https://doi.org/https://doi.org/10.1016/j.biortech.2018.12.075.

[3] M. Cerrillo, M. Vinas, A. Bonmatí, Startup of electromethanogenic microbial electrolysis cells with two different biomass inocula for biogas upgrading, ACS Sustain. Chem. Eng. 5 (2017) 8852–8859.

https://doi.org/10.1021/acssuschemeng.7b01636.

[4] M. Tabatabaei, M. Aghbashlo, E. Valijanian, H. Kazemi Shariat Panahi, A.-S. Nizami, H. Ghanavati, A. Sulaiman, S. Mirmohamadsadeghi, K. Karimi, A comprehensive review on recent biological innovations to improve biogas production, Part 2: Mainstream and downstream strategies, Renew. Energy. 146 (2020) 1392–1407. https://doi.org/https://doi.org/10.1016/j.renene.2019.07.047.

[5] T.W.M. Amen, O. Eljamal, A.M.E. Khalil, N. Matsunaga, Wastewater degradation by iron/copper nanoparticles and the microorganism growth rate, J. Environ. Sci. 74 (2018) 19–31. https://doi.org/https://doi.org/10.1016/j.jes.2018.01.028.

[6] M. Dehhaghi, M. Tabatabaei, M. Aghbashlo, H. Kazemi Shariat Panahi, A.-S. Nizami, A state-of-the-art review on the application of nanomaterials for enhancing biogas production, J. Environ. Manage. 251 (2019) 109597. https://doi.org/https://doi.org/10.1016/j.jenvman.2019.109597.

[7] A. Grosser, A. Grobelak, A. Rorat, P. Courtois, F. Vandenbulcke, S. Lemière, R. Guyoneaud, E. Attard, P. Celary, Effects of silver nanoparticles on performance of anaerobic digestion of sewage sludge and associated microbial communities, Renew. Energy. 171 (2021) 1014–1025. https://doi.org/https://doi.org/10.1016/j.renene.2021.02.127.

[8] M. Farghali, F.J. Andriamanohiarisoamanana, M.M. Ahmed, S. Kotb, T. Yamashiro, M. Iwasaki, K. Umetsu, Impacts of iron oxide and titanium dioxide nanoparticles on biogas production: Hydrogen sulfide mitigation, process stability, and prospective challenges, J. Environ. Manage. 240 (2019) 160–167. https://doi.org/10.1016/j.jenvman.2019.03.089.

[9] Z. Zhang, L. Guo, Y. Wang, Y. Zhao, Z. She, M. Gao, Y. Guo, Application of iron oxide (Fe3O4) nanoparticles during the two-stage anaerobic digestion with waste

sludge: Impact on the biogas production and the substrate metabolism, Renew. Energy. 146 (2020) 2724–2735. https://doi.org/https://doi.org/10.1016/j.renene.2019.08.078.

[10] P. Ghofrani-Isfahani, H. Baniamerian, P. Tsapekos, M. Alvarado-Morales, T. Kasama, M. Shahrokhi, M. Vossoughi, I. Angelidaki, Effect of metal oxide based TiO_2 nanoparticles on anaerobic digestion process of lignocellulosic substrate, Energy. 191 (2020) 116580. https://doi.org/https://doi.org/10.1016/j.energy.2019.116580.

[11] F. Suanon, Q. Sun, D. Mama, J. Li, B. Dimon, C.P. Yu, Effect of nanoscale zero-valent iron and magnetite (Fe_3O_4) on the fate of metals during anaerobic digestion of sludge, Water Res. 88 (2016) 897–903. https://doi.org/10.1016/j.watres.2015.11.014.

[12] G.S. Aguilar-Moreno, E. Navarro-Cerón, A. Velázquez-Hernández, G. Hernández-Eugenio, M.Á. Aguilar-Méndez, T. Espinosa-Solares, Enhancing methane yield of chicken litter in anaerobic digestion using magnetite nanoparticles, Renew. Energy. 147 (2020) 204–213. https://doi.org/https://doi.org/10.1016/j.renene.2019.08.111.

[13] C.-S. He, P.-P. He, H.-Y. Yang, L.-L. Li, Y. Lin, Y. Mu, H.-Q. Yu, Impact of zero-valent iron nanoparticles on the activity of anaerobic granular sludge: From macroscopic to microcosmic investigation, Water Res. 127 (2017) 32–40. https://doi.org/https://doi.org/10.1016/j.watres.2017.09.061.

[14] H. Mu, Y. Chen, Long-term effect of ZnO nanoparticles on waste activated sludge anaerobic digestion, Water Res. 45 (2011) 5612–5620. https://doi.org/https://doi.org/10.1016/j.watres.2011.08.022.

[15] Y. Yang, J. Guo, Z. Hu, Impact of nano zero valent iron (NZVI) on methanogenic activity and population dynamics in anaerobic digestion, Water Res. 47 (2013) 6790–6800. https://doi.org/https://doi.org/10.1016/j.watres.2013.09.012.

[16] J. Gonzalez-Estrella, R. Sierra-Alvarez, J.A. Field, Toxicity assessment of inorganic nanoparticles to acetoclastic and hydrogenotrophic methanogenic activity in anaerobic

granular sludge, J. Hazard. Mater. 260 (2013) 278–285. https://doi.org/https://doi.org/10.1016/j.jhazmat.2013.05.029.

[17] R. Barrena, E. Casals, J. Colón, X. Font, A. Sánchez, V. Puntes, Evaluation of the ecotoxicity of model nanoparticles, Chemosphere. 75 (2009) 850–857. https://doi.org/https://doi.org/10.1016/j.chemosphere.2009.01.078.

[18] M. Yazdani, M. Ebrahimi-Nik, A. Heidari, M.H. Abbaspour-Fard, Improvement of biogas production from slaughterhouse wastewater using biosynthesized iron nanoparticles from water treatment sludge, Renew. Energy. 135 (2019) 496–501. https://doi.org/https://doi.org/10.1016/j.renene.2018.12.019.

[19] B. Demirel, The impacts of engineered nanomaterials (ENMs) on anaerobic digestion processes, Process Biochem. 51 (2016) 308–313. https://doi.org/https://doi.org/10.1016/j.procbio.2015.12.007.

[20] Y.-J. Lee, D.-J. Lee, Impact of adding metal nanoparticles on anaerobic digestion performance – A review, Bioresour. Technol. 292 (2019) 121926. https://doi.org/https://doi.org/10.1016/j.biortech.2019.121926.

[21] E. Abdelsalam, M. Samer, Y.A. Attia, M.A. Abdel-Hadi, H.E. Hassan, Y. Badr, Influence of zero valent iron nanoparticles and magnetic iron oxide nanoparticles on biogas and methane production from anaerobic digestion of manure, Energy. 120 (2017) 842–853. https://doi.org/https://doi.org/10.1016/j.energy.2016.11.137.

[22] K. Bensaida, R. Eljamal, kareman Eljamal, Y. Sughihara, O. Eljamal, The impact of iron bimetallic nanoparticles on bulk microbial growth in wastewater, J. Water Process Eng. 40 (2021) 101825. https://doi.org/https://doi.org/10.1016/j.jwpe.2020.101825.

[23] E. Abdelsalam, M. Samer, Y.A. Attia, M.A. Abdel-Hadi, H.E. Hassan, Y. Badr, Comparison of nanoparticles effects on biogas and methane production from anaerobic digestion of cattle dung slurry, Renew. Energy. 87 (2016) 592–598.

731 https://doi.org/https://doi.org/10.1016/j.renene.2015.10.053.
732 [24] A. Hassanein, S. Lansing, R. Tikekar, Impact of metal nanoparticles on biogas
733 production from poultry litter, Bioresour. Technol. 275 (2019) 200–206.
734 https://doi.org/https://doi.org/10.1016/j.biortech.2018.12.048.
735 [25] W. Huang, F. Yang, W. Huang, Z. Lei, Z. Zhang, Enhancing hydrogenotrophic
736 activities by zero-valent iron addition as an effective method to improve sulfadiazine
737 removal during anaerobic digestion of swine manure, Bioresour. Technol. 294 (2019)
738 122178. https://doi.org/https://doi.org/10.1016/j.biortech.2019.122178.
739 [26] T.W.M. Amen, O. Eljamal, A.M.E. Khalil, Y. Sugihara, N. Matsunaga, Methane yield
740 enhancement by the addition of new novel of iron and copper-iron bimetallic
741 nanoparticles, Chem. Eng. Process. - Process Intensif. 130 (2018) 253–261.
742 https://doi.org/https://doi.org/10.1016/j.cep.2018.06.020.
743 [27] T. Jia, Z. Wang, H. Shan, Y. Liu, L. Gong, Effect of nanoscale zero-valent iron on
744 sludge anaerobic digestion, Resour. Conserv. Recycl. 127 (2017) 190–195.
745 https://doi.org/https://doi.org/10.1016/j.resconrec.2017.09.007.
746 [28] F. Suanon, Q. Sun, M. Li, X. Cai, Y. Zhang, Y. Yan, C.-P. Yu, Application of nanoscale
747 zero valent iron and iron powder during sludge anaerobic digestion: Impact on methane
748 yield and pharmaceutical and personal care products degradation, J. Hazard. Mater.
749 321 (2017) 47–53. https://doi.org/https://doi.org/10.1016/j.jhazmat.2016.08.076.
750 [29] J. Zhou, X. You, B. Niu, X. Yang, L. Gong, Y. Zhou, J. Wang, H. Zhang, Enhancement
751 of methanogenic activity in anaerobic digestion of high solids sludge by nano zero-
752 valent iron, Sci. Total Environ. 703 (2020) 135532.
753 https://doi.org/https://doi.org/10.1016/j.scitotenv.2019.135532.
754 [30] E. Kökdemir Ünşar, N.A. Perendeci, What kind of effects do Fe_2O_3 and Al_2O_3
755 nanoparticles have on anaerobic digestion, inhibition or enhancement?, Chemosphere.

211 (2018) 726–735. https://doi.org/https://doi.org/10.1016/j.chemosphere.2018.08.014.

[31] Y. Zhang, Z. Yang, R. Xu, Y. Xiang, M. Jia, J. Hu, Y. Zheng, W. Xiong, J. Cao, Enhanced mesophilic anaerobic digestion of waste sludge with the iron nanoparticles addition and kinetic analysis, Sci. Total Environ. 683 (2019) 124–133. https://doi.org/https://doi.org/10.1016/j.scitotenv.2019.05.214.

[32] Y. Zhang, Z. Yang, Y. Xiang, R. Xu, Y. Zheng, Y. Lu, M. Jia, S. Sun, J. Cao, W. Xiong, Evolutions of antibiotic resistance genes (ARGs), class 1 integron-integrase (intI1) and potential hosts of ARGs during sludge anaerobic digestion with the iron nanoparticles addition, Sci. Total Environ. 724 (2020) 138248. https://doi.org/https://doi.org/10.1016/j.scitotenv.2020.138248.

[33] S. Choe, S.-H. Lee, Y.-Y. Chang, K.-Y. Hwang, J. Khim, Rapid reductive destruction of hazardous organic compounds by nanoscale Fe_0, Chemosphere. 42 (2001) 367–372. https://doi.org/https://doi.org/10.1016/S0045-6535(00)00147-8.

[34] R. Barrena, M. del C. Vargas-García, G. Capell, M. Barańska, V. Puntes, J. Moral-Vico, A. Sánchez, X. Font, Sustained effect of zero-valent iron nanoparticles under semi-continuous anaerobic digestion of sewage sludge: Evolution of nanoparticles and microbial community dynamics, Sci. Total Environ. 777 (2021) 145969. https://doi.org/https://doi.org/10.1016/j.scitotenv.2021.145969.

[35] M. Cerrillo, L. Morey, M. Viñas, A. Bonmatí, Assessment of active methanogenic archaea in a methanol-fed upflow anaerobic sludge blanket reactor., Appl. Microbiol. Biotechnol. 100 (2016) 10137–10146. https://doi.org/10.1007/s00253-016-7862-4.

[36] APHA, Standard Methods for the Examination of Water and Wastewater, 20th ed., American Public Health Association, American Water Works Association, and Water Pollution Control Federation, Washington, D.C., 1999.

781 [37] G.K. Anderson, G. Yang, Determination of bicarbonate and total volatile acid
782 concentration in anaerobic digesters using a simple titration, Water Environ. Res. 64
783 (1992) 53–59. https://doi.org/https://doi.org/10.2175/WER.64.1.8.
784 [38] H. Tan, J. Verbeeck, A. Abakumov, G. Van Tendeloo, Oxidation state and chemical
785 shift investigation in transition metal oxides by EELS, Ultramicroscopy. 116 (2012)
786 24–33. https://doi.org/https://doi.org/10.1016/j.ultramic.2012.03.002.
787 [39] A.C. Lizama, C.C. Figueiras, A.Z. Pedreguera, J.E. Ruiz Espinoza, Enhancing the
788 performance and stability of the anaerobic digestion of sewage sludge by zero valent
789 iron nanoparticles dosage, Bioresour. Technol. 275 (2019) 352–359.
790 https://doi.org/https://doi.org/10.1016/j.biortech.2018.12.086.
791 [40] D. Wu, S. Zheng, A. Ding, G. Sun, M. Yang, Performance of a zero valent iron-based
792 anaerobic system in swine wastewater treatment, J. Hazard. Mater. 286 (2015) 1–6.
793 https://doi.org/https://doi.org/10.1016/j.jhazmat.2014.12.029.
794 [41] Y. Yang, F. Yang, W. Huang, W. Huang, F. Li, Z. Lei, Z. Zhang, Enhanced anaerobic
795 digestion of ammonia-rich swine manure by zero-valent iron: With special focus on
796 the enhancement effect on hydrogenotrophic methanogenesis activity, Bioresour.
797 Technol. 270 (2018) 172–179.
798 https://doi.org/https://doi.org/10.1016/j.biortech.2018.09.008.
799 [42] M. Cerrillo, M. Viñas, A. Bonmatí, Unravelling the active microbial community in a
800 thermophilic anaerobic digester-microbial electrolysis cell coupled system under
801 different conditions, Water Res. 110 (2017) 192–201.
802 https://doi.org/https://doi.org/10.1016/j.watres.2016.12.019.
803 [43] Y.-X. Huang, J. Guo, C. Zhang, Z. Hu, Hydrogen production from the dissolution of
804 nano zero valent iron and its effect on anaerobic digestion, Water Res. 88 (2016) 475–
805 480. https://doi.org/https://doi.org/10.1016/j.watres.2015.10.028.

[44] Y. Liu, H. Choi, D. Dionysiou, G. V Lowry, Trichloroethene Hydrodechlorination in Water by Highly Disordered Monometallic Nanoiron, Chem. Mater. 17 (2005) 5315–5322. https://doi.org/10.1021/cm0511217.

[45] Y. Liu, G. V. Lowry, Effect of particle age (Fe_0 content) and solution pH on NZVI reactivity: H2 evolution and TCE dechlorination, Environ. Sci. Technol. 40 (2006) 6085–6090. https://doi.org/10.1021/es060685o.

[46] D. Puyol, X. Flores-Alsina, Y. Segura, R. Molina, B. Padrino, J.L.G. Fierro, K. V Gernaey, J.A. Melero, F. Martinez, Exploring the effects of ZVI addition on resource recovery in the anaerobic digestion process, Chem. Eng. J. 335 (2018) 703–711. https://doi.org/https://doi.org/10.1016/j.cej.2017.11.029.

[47] G. Luo, I. Angelidaki, Co-digestion of manure and whey for in situ biogas upgrading by the addition of H2: process performance and microbial insights, Appl. Microbiol. Biotechnol. 97 (2013) 1373–1381. https://doi.org/10.1007/s00253-012-4547-5.

[48] G. Luo, S. Johansson, K. Boe, L. Xie, Q. Zhou, I. Angelidaki, Simultaneous hydrogen utilization and in situ biogas upgrading in an anaerobic reactor., Biotechnol. Bioeng. 109 (2012) 1088–1094. https://doi.org/10.1002/bit.24360.

[49] L. Liang, N. Korte, B. Gu, R. Puls, C. Reeter, Geochemical and microbial reactions affecting the long-term performance of in situ 'iron barriers,' Adv. Environ. Res. 4 (2000) 273–286. https://doi.org/https://doi.org/10.1016/S1093-0191(00)00026-5.

[50] K.-F. Chen, S. Li, W. Zhang, Renewable hydrogen generation by bimetallic zero valent iron nanoparticles, Chem. Eng. J. 170 (2011) 562–567. https://doi.org/https://doi.org/10.1016/j.cej.2010.12.019.

[51] I. Vyrides, M. Andronikou, A. Kyprianou, A. Modic, A. Filippeti, C. Yiakoumis, C.G. Samanides, CO_2 conversion to CH_4 using Zero Valent Iron (ZVI) and anaerobic granular sludge: Optimum batch conditions and microbial pathways, J. CO2 Util. 27

831 (2018) 415–422. https://doi.org/https://doi.org/10.1016/j.jcou.2018.08.023.
832 [52] A.-E. Rotaru, P.M. Shrestha, F. Liu, M. Shrestha, D. Shrestha, M. Embree, K. Zengler,
833 C. Wardman, K.P. Nevin, D.R. Lovley, A new model for electron flow during
834 anaerobic digestion: direct interspecies electron transfer to *Methanosaeta* for the
835 reduction of carbon dioxide to methane, Energy Environ. Sci. 7 (2014) 408–415.
836 https://doi.org/10.1039/C3EE42189A.
837 [53] S. Barua, B.R. Dhar, Advances towards understanding and engineering direct
838 interspecies electron transfer in anaerobic digestion, Bioresour. Technol. 244 (2017)
839 698–707. https://doi.org/https://doi.org/10.1016/j.biortech.2017.08.023.
840 [54] Z. Zhao, Y. Zhang, T.L. Woodard, K.P. Nevin, D.R. Lovley, Enhancing syntrophic
841 metabolism in up-flow anaerobic sludge blanket reactors with conductive carbon
842 materials, Bioresour. Technol. 191 (2015) 140–145.
843 https://doi.org/https://doi.org/10.1016/j.biortech.2015.05.007.
844 [55] Y. Dang, D.E. Holmes, Z. Zhao, T.L. Woodard, Y. Zhang, D. Sun, L.-Y. Wang, K.P.
845 Nevin, D.R. Lovley, Enhancing anaerobic digestion of complex organic waste with
846 carbon-based conductive materials, Bioresour. Technol. 220 (2016) 516–522.
847 https://doi.org/https://doi.org/10.1016/j.biortech.2016.08.114.
848 [56] F. Liu, A.-E. Rotaru, P.M. Shrestha, N.S. Malvankar, K.P. Nevin, D.R. Lovley,
849 Promoting direct interspecies electron transfer with activated carbon, Energy Environ.
850 Sci. 5 (2012) 8982–8989. https://doi.org/10.1039/C2EE22459C.
851 [57] J. Luo, L. Feng, Y. Chen, X. Li, H. Chen, N. Xiao, D. Wang, Stimulating short-chain
852 fatty acids production from waste activated sludge by nano zero-valent iron, J.
853 Biotechnol. 187 (2014) 98–105.
854 https://doi.org/https://doi.org/10.1016/j.jbiotec.2014.07.444.
855 [58] V. Domrongpokkaphan, C. Phalakornkule, M. Khemkhao, In-situ methane enrichment

of biogas from anaerobic digestion of palm oil mill effluent by addition of zero valent iron (ZVI), Int. J. Hydrogen Energy. (2021). https://doi.org/https://doi.org/10.1016/j.ijhydene.2021.03.083.

[59] F. He, D. Zhao, Hydrodechlorination of trichloroethene using stabilized Fe-Pd nanoparticles: Reaction mechanism and effects of stabilizers, catalysts and reaction conditions, Appl. Catal. B Environ. 84 (2008) 533–540. https://doi.org/https://doi.org/10.1016/j.apcatb.2008.05.008.

[60] F.S. dos Santos, F.R. Lago, L. Yokoyama, F.V. Fonseca, Synthesis and characterization of zero-valent iron nanoparticles supported on SBA-15, J. Mater. Res. Technol. 6 (2017) 178–183. https://doi.org/https://doi.org/10.1016/j.jmrt.2016.11.004.

[61] G. Zhen, X. Lu, Y.-Y. Li, Y. Liu, Y. Zhao, Influence of zero valent scrap iron (ZVSI) supply on methane production from waste activated sludge, Chem. Eng. J. 263 (2015) 461–470. https://doi.org/https://doi.org/10.1016/j.cej.2014.11.003.

[62] A. Liu, W. Zhang, Fine structural features of nanoscale zero-valent iron characterized by spherical aberration corrected scanning transmission electron microscopy (Cs-STEM), Analyst. 139 (2014) 4512–4518. https://doi.org/10.1039/C4AN00679H.

[63] H. Baniamerian, P.G. Isfahani, P. Tsapekos, M. Alvarado-Morales, M. Shahrokhi, M. Vossoughi, I. Angelidaki, Application of nano-structured materials in anaerobic digestion: Current status and perspectives, Chemosphere. 229 (2019) 188–199. https://doi.org/https://doi.org/10.1016/j.chemosphere.2019.04.193.

[64] F. Martins, S. Machado, T. Albergaria, C. Delerue-Matos, LCA applied to nano scale zero valent iron synthesis, Int. J. Life Cycle Assess. 22 (2017) 707–714. https://doi.org/10.1007/s11367-016-1258-7.

[65] S. Li, W. Yan, W. Zhang, Solvent-free production of nanoscale zero-valent iron (nZVI) with precision milling, Green Chem. 11 (2009) 1618–1626.

https://doi.org/10.1039/B913056J.

[66] O. Hijazi, E. Abdelsalam, M. Samer, Y.A. Attia, B.M.A. Amer, M.A. Amer, M. Badr, H. Bernhardt, Life cycle assessment of the use of nanomaterials in biogas production from anaerobic digestion of manure, Renew. Energy. 148 (2020) 417–424. https://doi.org/https://doi.org/10.1016/j.renene.2019.10.048.